Far-infrared optical properties of semiconducting tetrathiafulvalene tetracyanoquinodimethane (TTF-TCNQ), including the pinned charge-density wave

J. E. Eldridge and Frances E. Bates
Department of Physics, University of British Columbia, Vancouver, British Columbia V6T 1W5, Canada
(Received 9 September 1982; revised manuscript received 23 August 1983)

The far-infrared bolometric response of a thick single crystal of TTF-TCNQ at 12 K has been used to give directly $1-R$, where R is the power reflectivity, for radiation polarized with $\vec{E}||\vec{b}$, and wave numbers from 10 to 830 cm^{-1}. Accurate and high-resolution values of R are obtained. These have been combined with measurements at higher energies and a Kramers-Kronig analysis performed to yield the optical properties. The conductivity shows a strong resonance at 35 cm^{-1}, which has been attributed to the phase mode of the pinned charge-density wave, in agreement with Tanner, Cummings, and Jacobsen [Phys. Rev. Lett. 47, 597 (1981)]. We find, however, no large resonance at higher wave numbers but instead a strong broad midgap conductivity possibly attributable to solitons. The optical properties are confirmed by comparison with powder transmission measurements. The effect of small particles on the powder and thin-film spectra is demonstrated. Finally, temperature-dependent powder measurements have been used to show the activated nature of the anomalous $\vec{E}||\vec{b}$ vibrational spectrum.

I. INTRODUCTION

Recently Tanner, Cummings, and Jacobsen[1] measured the far-infrared reflectivity from a mosaic of tetrathiafulvalene tetracyanoquinodimethane (TTF-TCNQ) single crystals at several temperatures. A Kramers-Kronig analysis of the measured spectrum at 25 K yielded a conductivity which contained a strong feature around 40 cm^{-1}, which was assigned to the pinned charge-density wave (CDW), and a much stronger feature around 290 cm^{-1}, which was unassigned. The CDW at 40 cm^{-1} was in disagreement with our interpretation of the bolometric spectrum, which gave a pinning frequency[2] of 3.4 cm^{-1}, and the strong 290-cm^{-1} feature was also in disagreement with our bolometric spectra[3-6] and various other measurements of far-infrared transmission through powders.[7-9] Our interpretation[2] of the bolometric spectrum had been that for $\vec{E}||\vec{b}$, where $\vec{b}$ is the high-temperature conducting direction, the bolometric signal saturates to $1-R$, where R is the reflectivity, at the pinned CDW and above the semiconducting gap, but that in the gap the spectrum contained absorption features. Tanner *et al.*[1] suggested that, on the contrary, the entire spectrum was saturating to $1-R$, in which case our reflectivity resembled that measured directly by them. We have determined that this is indeed the case. Our technique, however, has allowed us to obtain the very high reflectivity more accurately than is possible by a direct method with a mosaic of single crystals, and our resulting conductivity spectrum, while now agreeing with the pinned CDW around 35 cm^{-1} as measured by Tanner, does not contain the very strong 290-cm^{-1} feature. We also find the CDW to have a larger oscillator strength than that reported by Tanner, with a corresponding decrease in effective mass, and we speculate that solitons may be responsible for the very high conductivity in the semiconducting gap.

Another difficulty with the far-infrared properties of TTF-TCNQ over the last few years has been the interpretation of the powder spectra. Why has the pinned CDW at 33—40 cm^{-1} not been observed in powder absorption, which instead seems to give a broad CDW with a pinning frequency[7] of 80 cm^{-1}? Why did the powder spectra seem to indicate a semiconducting energy gap at all temperatures,[7] while this is known not to be the case? We have used the reflectivity spectrum obtained by the bolometric technique to generate all of the various optical properties, including the absorption coefficient of the powders. By including small-particle effects it has been possible to reproduce, with good agreement, both the high-resolution far-infrared powder spectra of our own, presented here for the first time, and the general features of the thin-film data of Tanner *et al.*[7] Thus, the questions just raised can be satisfactorily answered.

With the powder spectrum understood it became possible to identify features in the necessarily unpolarized powder absorption with those which have been studied in great detail in the polarized bolometric spectra.[3] In particular, many vibrational features in the $\vec{E}||\vec{b}$ spectrum, which have been assigned to librations and other normally infrared-inactive modes, were predicted to be activated at low temperatures by coupling with the CDW due to the Peierls distortion. It was, however, impossible to test this prediction with the bolometric technique since it works only at low temperatures. Here we will present powder spectra at different temperatures which will confirm the activated nature of these anomalous absorption features.

II. OPTICAL PROPERTIES

The full curves in Figs. 1 and 2 show portions of the 12-K bolometric spectra obtained from a single crystal of

TTF-TCNQ approximately 30 μm thick, for radiation polarized with $\vec{E}||\vec{a}$ and $\vec{E}||\vec{b}$, respectively. Reference 3 contains both high-resolution spectra of this region together with lower-resolution spectra up to 900 cm^{-1}. It also contains a derivation of the expression for I_A/I_0, the intensity absorbed, relative to that incident on the crystal, which produces the bolometric signal, in terms of the power reflectivity R, the absorption coefficient α, and the average crystal thickness d. The equation is reproduced here as follows:

$$\frac{I_A}{I_0}=\frac{(1-R)+(2R-1-4R\sin^2\psi)e^{-\alpha d}-Re^{-2\alpha d}-R^2e^{-\alpha d}(1-e^{-\alpha d})}{1-R^2e^{-2\alpha d}}, \tag{1}$$

where

$$\tan\psi=2k/(n^2+k^2-1). \tag{2}$$

Figure 2 in Ref. 3 shows the behavior of this expression as a function of αd, which is in effect to "saturate" to $1-R$ as αd becomes very large. This is the expected result when no radiation is transmitted through the sample, since the absorbed intensity is then simply that which is incident minus that which is reflected. Some of the absorption features in the $\vec{E}||\vec{a}$ spectrum are sufficiently strong to saturate at the peaks, and this produced false structure in the bolometric spectrum resulting from the dips in the reflectivity, which is well described in Fig. 9 of Ref. 3.

Because of the very high reflectivity in the $\vec{E}||\vec{b}$ polarization,[10] however, which would be unaffected by vibrational modes of the usual strength, and because of the anticipated low absorption in the semiconducting gap, the $\vec{E}||\vec{b}$ spectrum between 30 and 300 cm^{-1} was attributed to absorption features. Further support for this interpretation was given in Ref. 3. The recent reflectivity measurement by Tanner *et al.*,[1] however, prompted us to investigate further. We decided to obtain a bolometric spectrum from a *very* thick crystal through which the $\vec{E}||\vec{b}$ radiation would have little chance of passing, giving a signal almost certainly proportional to $1-R$. The dashed curve in Fig. 1 is the result for $\vec{E}||\vec{a}$ with a 200-μm-thick crystal. The signal is considerably increased from the 30-μm-thick case, as expected from the increased thickness and absorption, except at the peaks, and false dip at 122 cm^{-1}, where it was already known to be saturated. Figure 2 shows the corresponding spectra for $\vec{E}||\vec{b}$. It is apparent that there is very little difference from the 30-μm-thick spectrum and the many sharp features remain. *Consequently, the many sharp features and detailed structure seen in the $\vec{E}||\vec{b}$ bolometric spectrum are due to the reflectivity and not the absorption coefficient, as supposed earlier.*

It is important for us to emphasize a few points at this juncture. The recent vibrational analysis[3] performed by us, involving the measurement of small frequency shifts upon deuterating the compound, as well as the comparison with the tetraselenafulvalene tetracyanoquinodimethane (TSeF-TCNQ) spectra, is still completely valid.

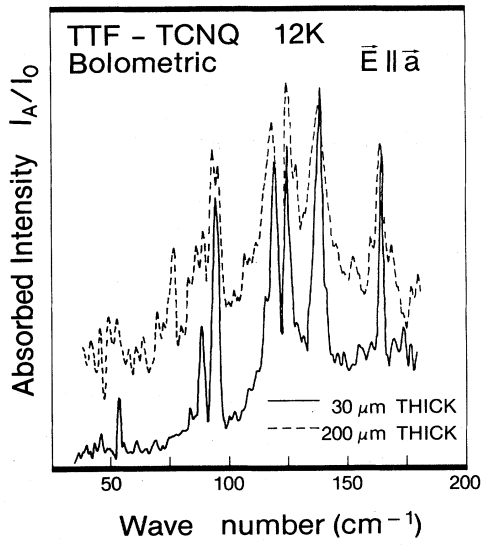

FIG. 1. 12-K bolometric spectra of TTF-TCNQ for $\vec{E}||\vec{a}$ obtained from two single crystals, one 30 μm thick and the other 200 μm thick. Expression for I_A/I_0 is given in the text. Notice the increased signal from the thicker crystal, demonstrating that it is proportional to absorption coefficient. Spectra saturate to $1-R$ near the resonance peaks, and this is the cause of the false dip at 122 cm^{-1}, where the full and dashed lines coincide.

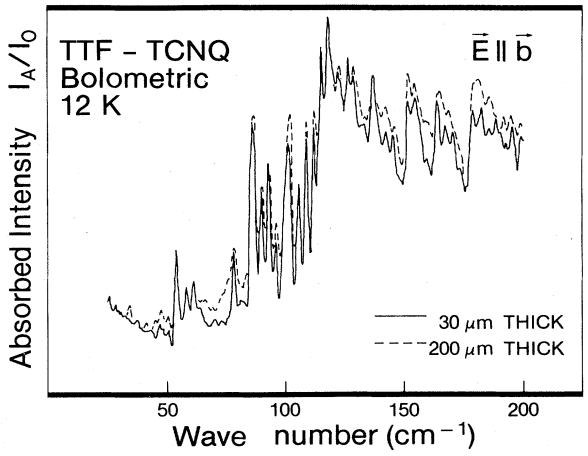

FIG. 2. 12-K bolometric spectra of TTF-TCNQ for $\vec{E}||\vec{b}$, obtained from two single crystals, one 30 μm thick and the other 200 μm thick. Expression for I_A/I_0 is given in the text. Notice the little difference between the two spectra, indicating that for both crystals the spectra are proportional to $1-R$.

It makes no difference whether we measure the absorption or reflectivity features. The earlier experiment to suppress the bolometric response relative to the photoconductive response in order to obtain the semiconducting energy-band gap[5] also remains valid, and the gap of approximately 300 cm^{-1} is unchanged. Our earlier interpretation[2] of the rise in the bolometric spectrum around 10 cm^{-1} to yield a CDW pinned at 3.4 cm^{-1} is, however, invalid. It is also clear that the vibrational modes which are so affecting the reflectivity are extremely strong and must therefore be coupling with the CDW.

The $\vec{E}||\vec{b}$ bolometric spectrum from the 200-μm-thick crystal is unquestionably proportional to $1-R$. Since R is so large, the technique is therefore a very powerful one for obtaining the small difference between R and unity. We have measured the spectrum up to 830 cm^{-1} and our resulting reflectivity is shown in Fig. 3. This spectrum was calibrated by two independent methods. The first was to match it to the directly measured reflectivity from 830 to 8000 cm^{-1} at 15 K from Jacobsen.[11] The second method was to compare the $\vec{E}||\vec{a}$ and $\vec{E}||\vec{b}$ bolometric responses between 500 and 900 cm^{-1}, a region in which they are both saturated to $1-R$. Taking the $\vec{E}||\vec{a}$ reflectivity[7] to be 0.14, we obtained an average value of 0.86 for $R(\vec{E}||\vec{b})$ between 500 and 900 cm^{-1}, which agrees with Fig. 3. The polarizers used were from Cambridge Physical Sciences. A KRS-5 substrate model with a 99% degree of polarization was used above 300 cm^{-1}, and a polyester model with 93% polarization was used below 300 cm^{-1}. The Mylar beam splitters provided an additional 75% $\vec{E}||\vec{b}$ polarization. These were placed just before the sample chamber of a Research and Industrial Instruments Company model no. FS-720 Michelson-type Fourier spectrometer in which the sample was mounted on a cold finger. A wedge-shaped light guide immediately in front of the sample provided some focusing without destroying the polarization.

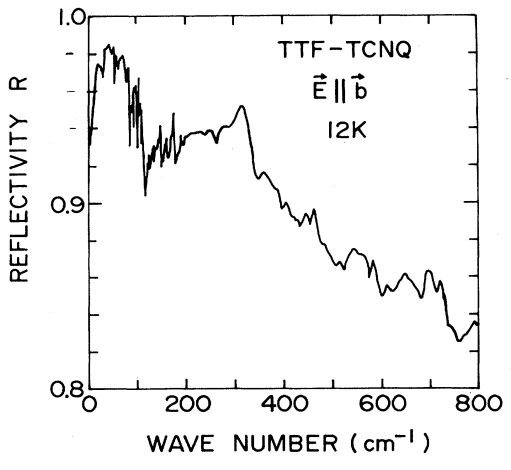

FIG. 3. Power reflectivity of TTF-TCNQ at 12 K for $\vec{E}||\vec{b}$ derived from the bolometric spectrum. Resolution is 1 cm^{-1} up to 200 cm^{-1} and 5 cm^{-1} from 200 to 800 cm^{-1}. Notice the suppressed zero.

The background spectra were obtained with a Golay detector with a diamond window which has a flat response from 10 to 1000 cm^{-1}, apart from a 12% broad transmission dip around 500 cm^{-1} due to the diamond. The measurements were taken at a fairly high sample temperature ($\sim$12 K) and with a low chopping frequency in order to maximize the bolometric response relative to any photoconductive response which would contribute to the signal above the band gap of about 300 cm^{-1}. The photoconductive response was estimated to be less than 4% of the total[12] in this region. The photogenerated carriers rapidly decay mainly by phonon emission, thereby heating the crystal and causing a bolometric response, as obtained below the gap. Further experimental details may be found in Ref. 3.

The high value of the reflectivity in Fig. 3 should be noted and the spectrum compared with that obtained by Tanner *et al.*[1] Many features are common to the two spectra: dips at 10, 90, 120, 180, 260, 350, 450, and 600 cm^{-1}, and broad peaks around 80 and 320 cm^{-1}. The main disagreements are in the magnitude or absolute value of R, which is so important when R is so large and a Kramers-Kronig analysis is to be performed. We find the 120-cm^{-1} dip to extend only to 0.9 rather than 0.8, and for R to drop gradually but fairly constantly from 0.94 at 300 cm^{-1} to 0.84 at 800 cm^{-1}, where it has been matched to the value of Jacobsen. In contrast, the reflectivity in Ref. 1 climbs after 300 cm^{-1} to a value of unity at 600 cm^{-1}. These are the causes of the main difference between the conductivity spectrum we will obtain and that presented by Tanner *et al.* Their work consisted of a direct measurement of reflectivity from a mosaic of crystals, which was then coated with evaporated gold, and replaced in the cryostat to give a reference spectrum. This is a very difficult experiment in which a small error in the absolute magnitude is not unexpected.

Above 8000 cm^{-1} we used the room-temperature data from Grant *et al.*,[13] which extended to 36000 cm^{-1}. In Fig. 4 we show, on a logarithmic frequency scale, the resulting reflectivity curve up to 10000 cm^{-1}, just beyond the plasma edge. (This frequency range is a good one to show the powder absorption later.) We performed a standard Kramers-Kronig analysis. Above 36000 cm^{-1} the value of R was assumed constant. This allows the Kramers-Kronig integral to be easily solved[14] and gives a high-frequency correction to the phase angle θ which is obtained in the analysis. This correction is very small for wave numbers in the far infrared. A low-frequency extrapolation below 10 cm^{-1}, where we were unable to measure, was also required. The optical properties in this region however are very sensitive to the extrapolation chosen. The dip in reflectivity below 50 cm^{-1} seen in Fig. 3 is believed to be real and not due to a decrease in the Golay response, simply because it is seen only for $\vec{E}||\vec{b}$ and not for $\vec{E}\perp\vec{b}$.[3] (It is also seen in Ref. 1.) We have therefore linearly extrapolated this decrease below 10 cm^{-1} to a value of 0.93 at zero frequency. This gives a static real part of the dielectric constant $\epsilon_1(0)$ equal to 3000, in agreement with the measured microwave values. Unfortunately this extrapolation gives very small but neg-

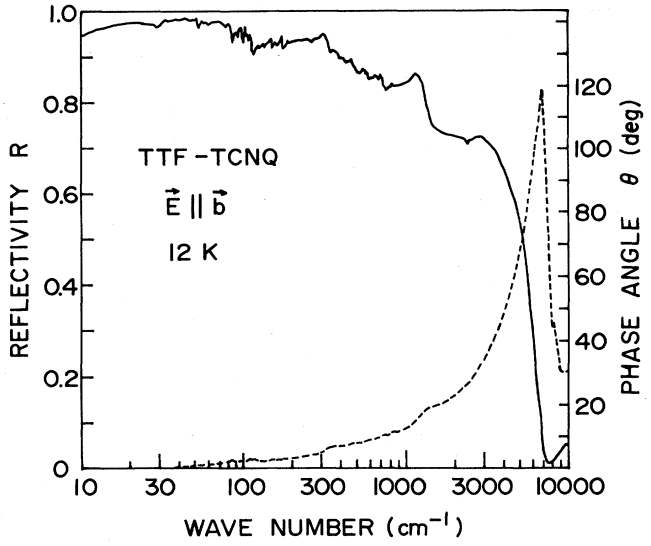

FIG. 4. Solid curve is the power reflectivity of TTF-TCNQ at 12 K for $\vec{E}||\vec{b}$ up to just beyond the plasma frequency on a logarithmic frequency scale. Values up to 830 cm^{-1} were obtained from the bolometric spectrum: 830–8000 cm^{-1} from Ref. 11 with 83-cm^{-1} resolution and above 8000 cm^{-1} from Ref. 13 with 800-cm^{-1} resolution. Dashed curve is the phase angle θ obtained from a Kramers-Kronig integral of the reflectivity.

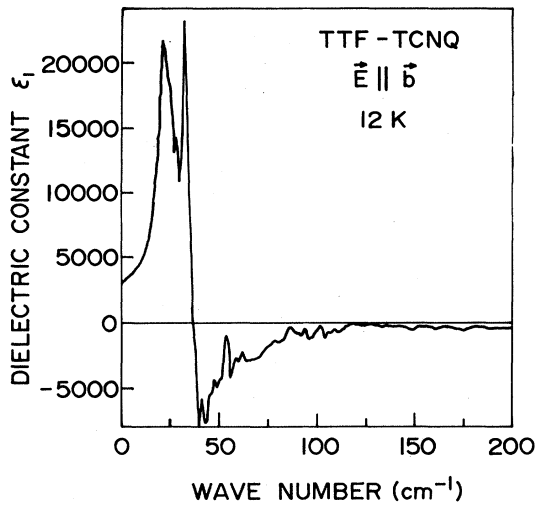

FIG. 5. Real part of the dielectric constant ϵ_1 of TTF-TCNQ at 12 K for $\vec{E}||\vec{b}$ in the region of the pinned CDW. Above 200 cm^{-1} it continues to be relatively small and negative until the plasma frequency near 7500 cm^{-1}.

ative values of θ below 20 cm^{-1} with a minimum of $-0.45°$ at 10 cm^{-1} (see Fig. 4 for a plot of θ from 10 to 10000 cm^{-1}). This produces nonphysical negative values of conductivity in this region. This, however, is thought to be due to errors of a few percent in the reflectivity somewhere in the entire spectrum, which corresponds to the accuracy of the various experimental results. Initially negative values of θ are a common indication of incorrect high-frequency extrapolations or small errors in the measured value of R when R *increases* with frequency from the origin. A low-frequency extrapolation which would keep the conductivity positive below 20 cm^{-1} would give a value of $\epsilon_1(0)$ equal to 8000, which is almost certainly too high.

The low-wave-number form of $\epsilon_1(\bar{\nu})$ may be seen in Fig. 5. It is similar to that obtained by Tanner except that it has larger extreme values, both positive and negative, and then remains small and negative until $n=k$ at the plasma edge near 7500 cm^{-1}.

The imaginary part of the dielectric constant has not been presented since it contains the same information as the conductivity, given in units of $\Omega^{-1}\,cm^{-1}$ by

$$\sigma=\frac{nk\bar{\nu}}{30}\,, \tag{3}$$

where n and k are the refractive index and extinction coefficient, respectively, both of which were obtained from R and θ, and $\bar{\nu}$ is in wave numbers. Figure 6 shows the conductivity up to 500 cm^{-1}. The large lower resonance with a peak between 33 and 35 cm^{-1} is identified as the pinned CDW. It is close in pinning frequency to that reported by Tanner, but has more than twice the oscillator strength. While the pinning frequency remains constant, the width and strength of the peak are sensitive to the low-frequency R extrapolation. It may be seen that there is no large resonance near 290 cm^{-1} as found by Tanner. Instead we have very high conductivity in the band gap (below 315 cm^{-1}) with an increase following the CDW starting just about 100 cm^{-1}. The conductivity above the gap in Fig. 6

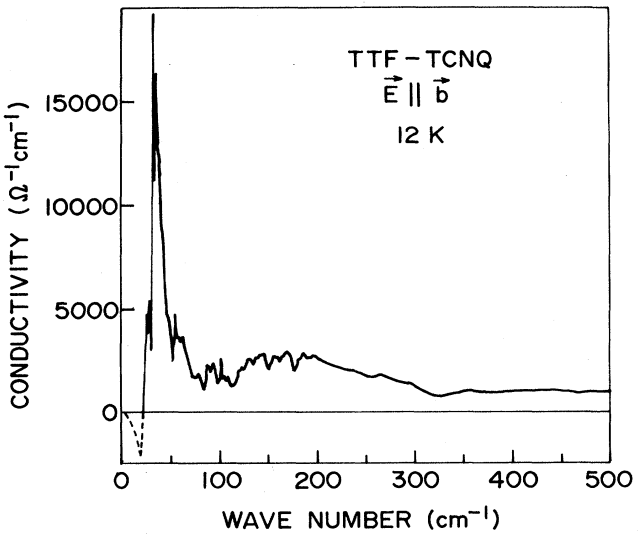

FIG. 6. Conductivity σ of TTF-TCNQ at 12 K for $\vec{E}||\vec{b}$. Strong sharp feature at 35 cm^{-1} is identified as the phase mode of the pinned CDW. Notice the strong conductivity in the gap below 315 cm^{-1}.

is about 1000 $\Omega^{-1}\,\mathrm{cm}^{-1}$, approximately the same as the peak value at room temperature,[7] but we must admit that it is so small in comparison with the conductivity in the gap that it does not resemble a gap at all. The cause and strength of the midgap absorption must surely be related to the pinned CDW at lower energy. The dip at 320 cm^{-1} which seems to coincide with the gap edge has been assigned to an activated vibrational mode[8,9] even though it is so much wider than the others observed. The absorption coefficient to be presented in Sec. III, however, resembles more closely that expected for a semiconductor, with the absorption above the energy gap being greater than that below. We next examine the question of solitons in the gap.

The oscillator-strength sum rule in our units ($\Omega^{-1}\,\mathrm{cm}^{-1}$) can be written

$$\Omega_p^2=\frac{120}{\pi}\int_0^{84\,\mathrm{cm}^{-1}}\sigma\,d\bar{\nu}\ . \tag{4}$$

Integrating to the dip at 84 cm^{-1} gives $\Omega_p=3270$ cm^{-1}. Again, in our units (Ω_p in units of cm^{-1}), one can write

$$\Omega_p^2=\frac{1}{(2\pi c)^2}\frac{4\pi n e^2 m_e}{VM^*}\ , \tag{5}$$

where m_e is the electronic mass, n is the combined electron-hole densities per unit volume (equal to 2.4 for 0.6 charge transfer with $V=840$ Å^3), and M^* is the pinned-mode effective mass. This gives $M^*=24m_e$, even lighter than that found by Tanner. Taking an average of the TCNQ-band effective mass of 2.4 and the TTF-band effective mass of 5.2, one has $m_e^*=3.8m_e$, which gives $M^*=6.3m_e^*$. A fairly large uncertainty, say 30%, can be associated with these numbers due to the low-frequency extrapolation of R.

Rice *et al.*[15] predicted the existence of new, nonlinear, current-carrying elementary excitations, known as "ϕ" particles or "solitons," to occur with weakly pinned CDW's. Berlinsky[16] has considered these excitations in his review on CDW effects. In contrast to the small-amplitude phase oscillations of the CDW condensate, which is responsible for the large conductivity peak at 35 cm^{-1}, the solitons involve large changes in the phase and are confined to a finite region which propagates down the chain with a well-defined velocity. Physically they correspond to propagating compressions or rarefactions of the combined electron density, separating segments having common uniform phase and acting rather like domain walls. The minimum energy[15,16] required to create a soliton is E_0 where

$$E_0=\frac{4}{\pi}(m^*/m_e^*)^{1/2}\bar{\nu}_T \tag{6}$$

and $\bar{\nu}_T$ is the pinning frequency of 35 cm^{-1}. This gives $E_0=112$ cm^{-1}. Optically, however, one would need to create a soliton-antisoliton pair which has a threshold energy of $2E_0=224$ cm^{-1}. Above this one would expect a continuum of conductivity due to this process until the energy-band edge is reached. This may explain the high end of the midgap conductivity in Fig. 6.

If the 35-cm^{-1} mode is a phase oscillation of the CDW which is pinned by a cosine potential due to the Coulomb attraction between oppositely charged chains, then one has to consider all of the solutions of the sine-Gordon equation. Above $\bar{\nu}_T$ and below $2E_0$ there will be discrete solutions representing various orders of "breather" modes of soliton-antisoliton pairs, of which the strong mode at $\bar{\nu}_T$ is the first.[17] Calculations of the strength and energy of these modes are currently in progress[18] in order to see whether these contribute to the conductivity in this region.

III. COMPARISON WITH POWDER SPECTRA

When one obtains such "unusual" results for the optical properties of a compound, it is natural to try to confirm them with another technique. The absorption and reflectivity are both too strong for transmission studies through single crystals, and so we have looked at fine powders. As mentioned in the Introduction several questions also need to be answered concerning the results one obtains with powders and films.

Experimentally we performed the powder measurements much as Bozio and Pecile[9] have done. A few crystals are ground in Nujol mull for 15 or 20 min and the mixture is then applied to a wedged TPX (TPX is the Mitsui and Co., Ltd. trademark for methyl-pentene polymer) or polyethylene window. The window is then inserted into our Janis Supervaritemp Dewar in which the cooling is achieved by helium gas. The temperature is known to well within a degree and can be controlled with comparable accuracy. The samples were found to not cycle very well and so fresh ones were prepared for each run. The absorption depended, of course, on the amount of material on the window. Our spectra extended only to 300 cm^{-1} since low-temperature powder-absorption data above this frequency already exist.[8,9]

The solid curve in Fig. 7 shows, over the same logarithmic frequency scale, the absorption coefficient α given by

$$\alpha=4\pi k\,\bar{\nu}=4\pi\bar{\nu}\left[\frac{|\hat{\epsilon}|-\epsilon_1}{2}\right]^{1/2}\ , \tag{7}$$

which is the appropriate expression for the *bulk* material. *It is immediately apparent that the pinned CDW does not stand out as clearly in α as it does in the conductivity.* This is because α is proportional to σ divided by n, and n is very large at the low end of the spectrum. The CDW is nevertheless responsible for the broad absorption feature between 30 and 100 cm^{-1}. This is not seen, however, in either our present powder measurements or in the thin-film data of Tanner *et al.*[7] Our measured powder spectrum in this region is plotted as the upper trace in Fig. 8. Instead, this shows absorption which is low at 30 cm^{-1} and increases to a gentle maximum around 100 cm^{-1}. Figure 14 of Tanner[7] shows a more pronounced broad feature centered around 80 cm^{-1}. It is now clear that these do result from the pinned CDW, but small-particle effects (or Rayleigh absorption) are responsible for masking the CDW and shifting the absorption peak to higher frequencies.

There are various starting points and formalisms for the attenuation produced by small particles, but we will use

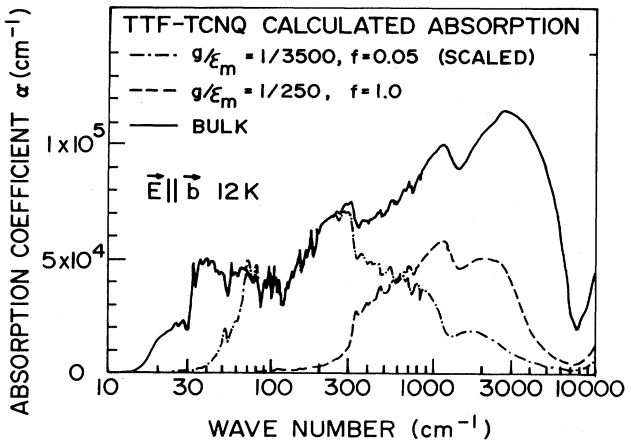

FIG. 7. Absorption coefficient α of TTF-TCNQ at 12 K for $\vec{E}||\vec{b}$. Curve for the bulk material was calculated from Eq. (7) using the dielectric constants from Figs. 5 and 6. Other two curves were calculated from Eqs. (8)—(10) using the same dielectric constants. Dashed curve is the thin-film absorption coefficient with $g/\epsilon_m=\frac{1}{250}$ and a filling factor of unity. Dotted-dashed curve applies to one of our Nujol mull powders with $g/\epsilon_m=\frac{1}{3500}$ and a filling factor of 0.05. This spectrum has been arbitrarily scaled up by a factor of 8 to match the bulk case in the region of agreement.

the results obtained by Tanner and Jacobsen,[7] modified for powder particles in an oil mull in which the filling factor f is small. We have also preferred to work with both parts of the dielectric constant rather than using the conductivity. Starting then with Eq. (11) of Ref. 7 one obtains, for the average dielectric constants of the powder,

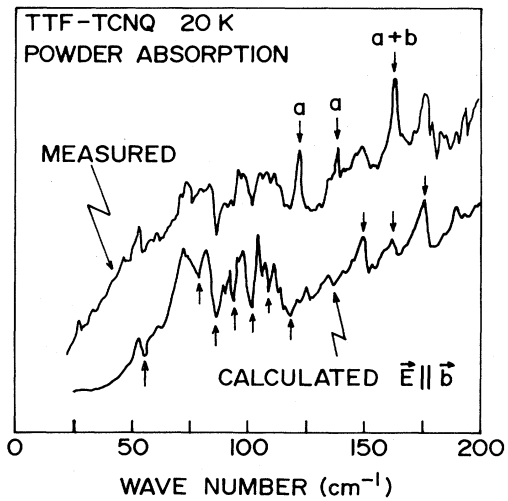

FIG. 8. Measured and calculated absorption coefficient of TTF-TCNQ at 20 K up to 200 cm^{-1}. Measured spectrum is $\ln(I_0/I)$. Calculated spectrum was obtained from Fig. 7 with $g/\epsilon_m=\frac{1}{3500}$ and $f=0.05$. Features seen for $\vec{E}||\vec{a}$ are so indicated. $\vec{E}||\vec{b}$ features common to the two spectra are also indicated. Two spectra have been vertically displaced for ease of comparison.

$$\langle\epsilon_2^b\rangle=\frac{f}{3}\frac{\epsilon_2^b}{[1+(g\epsilon_1^b/\epsilon_m)]^2+(g\epsilon_2^b/\epsilon_m)^2}\,, \tag{8}$$

and

$$\langle\epsilon_1^b\rangle=\epsilon_m+\frac{f}{3}\left[\frac{\epsilon_1^b+\{g[(\epsilon_1^b)^2+(\epsilon_2^b)^2]/\epsilon_m\}}{[1+(g\epsilon_1^b/\epsilon_m)]^2+(g\epsilon_2^b/\epsilon_m)^2}\right], \tag{9}$$

where g is the depolarization factor of the particles, f is the filling factor (volume fraction of crystals in the medium), and ϵ_m is the real dielectric constant of the medium. In the thin-film case ϵ_m is a composite of the $\vec{E}\perp\vec{b}$ dielectric constant of the crystals and that of free space. In our case it is a composite of this $\vec{E}\perp\vec{b}$ value, approximately 5, and the dielectric constant of Nujol mull, equal to 2.15. Equations (8) and (9) assume that $\epsilon_2^b\gg\epsilon_2^a$ and ϵ_2^c. This is a correct assumption in our experimental region with ϵ_2^b rising from 350 at 300 cm^{-1} to 35 000 at 33 cm^{-1}, while ϵ_2^a is only about 25 at the peak of the strongest feature,[3] 120 cm^{-1}. This does not, however, mean that $\vec{E}\perp\vec{b}$ features should not be expected in the powder-absorption spectrum. They will be seen because once again α is proportional to ϵ_2 divided by n and n is large for $\vec{E}||\vec{b}$. As given in Ref. 7, g varies between zero for a long needle particle and unity for a slab.

The $\vec{E}||\vec{b}$ absorption coefficient of the powders is then given by

$$\alpha^b=4\pi\bar{\nu}\left[\frac{|\langle\hat{\epsilon}^b\rangle|-\langle\epsilon_1^b\rangle}{2}\right]^{1/2} \tag{10}$$

and calculated using both Eqs. (8) and (9) to give the complex value $\langle\hat{\epsilon}^b\rangle$. This is important since, if one assumes that the absorption is merely proportional to σ or ϵ_2 and uses Eq. (8) alone, one then has the problem of a false "resonance" produced when $g\epsilon_1^b/\epsilon_m$ equals -1, remembering that ϵ_1^b is negative.

Figure 7 shows, along with the bulk absorption coefficient, two cases of powder absorption. The dashed curve applies to the thin-film case with a filling factor of approximately unity and a value of $g/\epsilon_m=\frac{1}{250}$, since the films consisted of crystallites with relative dimensions, which if assumed to be ellipsoidal, gave $g=\frac{1}{100}$. This should be compared with the 4-K curve in Fig. 13 of Ref. 7. The agreement is excellent both in shape and magnitude. Note the maximum of 6×10^4, down from 10^5 for the bulk case (see Fig. 12 of Ref. 7). Notice also the attenuation of the maximum between 2000 and 3000 cm^{-1} relative to the 1000-cm^{-1} peak, which is mainly due to the $f/3$ factor. The most dramatic effect is, however, the steep cutoff below 300 cm^{-1} which is due to the small-particle effects with $g/\epsilon_m=\frac{1}{250}$, since the cutoff occurs where $g/\epsilon_m\approx1/\epsilon_2^b$. This suppressed absorption at all temperatures led to the erroneous assumption of an energy gap at all temperatures.

Figure 8 shows our measured powder spectrum in the range 25—200 cm^{-1}. The calculated absorption with $g/\epsilon_m=\frac{1}{250}$ does not agree with this spectrum. Instead the best agreement in overall shape of the spectra is obtained with $g/\epsilon_m=\frac{1}{3500}$ and the resulting calculated spectrum is

shown in both Figs. 7 and 8. In Fig. 7 this has been arbitrarily scaled to match the bulk absorption coefficient in the region of agreement. Above this region, which ends at approximately 300 cm^{-1}, the absorption is strongly reduced due to the filling factor (i.e., when $\epsilon_m \approx f\epsilon_2^b/3$). The value of $f=0.05$ used in the calculation was the approximate value of our mulls when freshly prepared. The Nujol evaporates in time, increasing the value of f.

It may be seen that the cutoff due to small-particle effects, which now occurs when $\epsilon_2^b \approx 3500$, suppresses the low-energy CDW absorption below about 50 cm^{-1} and produces a very broad absorption feature centered around 90 cm^{-1} or so. This also agrees with the thin-film data in this region. Why is the depolarization factor so much lower in this region? It is most probably due to the interaction between particles as outlined by Tanner *et al.*[7] The dipole fields due to neighboring particles can be greater than the external field and so they suppress the small-particle effects. In this wave-number region the absorption is low and so both the powder and the thin-film samples are thick and such interaction is enhanced. (The thin-film data from 300 to 4000 cm^{-1} was obtained from very thin films in which such interaction would be small and the expected depolarization factor would apply.) The agreement in Fig. 8 between the experimental and calculated fine structure may also be seen to be very good. All of this structure has been studied in detail and most of it assigned to various vibrational modes.[3] Arrows on the calculated spectrum indicate some of the $\vec{E}||\vec{b}$ features which are observed experimentally.

When we first studied the isotope-induced frequency shifts of the features in the bolometric spectrum,[3] it was not clear whether we should have identified the peaks or the dips. We therefore chose the sharpest features. These have mostly turned out to be antiresonance *dips* in the conductivity of Fig. 6, while in both the reflectivity and absorption coefficients, they are *peaks* above 120 cm^{-1} and *dips* below 120 cm^{-1}. This is because of the large negative value of ϵ_1^b below 120 cm^{-1}, as seen in Fig. 5. Once again the importance of calculating α from Eq. (10) is emphasized since Eq. (8) alone would give inverted absorption features below 120 cm^{-1}. The $\vec{E}||\vec{a}$ experimental features, which are obviously missing from the calculation, are also indicated in Fig. 8.[19]

The features indicated with an arrow in Fig. 8 are the large ones, yet we also find agreement with the much smaller ones. Figure 9 is a similar plot of an expanded section from 90 to 130 cm^{-1}, and once again arrows show the excellent agreement between the powder spectrum and that calculated using the bolometric data as input. The bolometric spectra were taken with 0.5-cm^{-1} resolution. For the Kramers-Kronig analysis, however, points were taken only every 1 cm^{-1}. This is why the calculated curve in Fig. 9 is disjointed.

The upper end of our powder measurements, 100—330 cm^{-1}, is shown in Fig. 10, with lower resolution. The sample used to obtain this spectrum had to have less powder present than that used for Fig. 9 due to the higher absorption, and we again found that the effective depolarization had changed. The best agreement was obtained

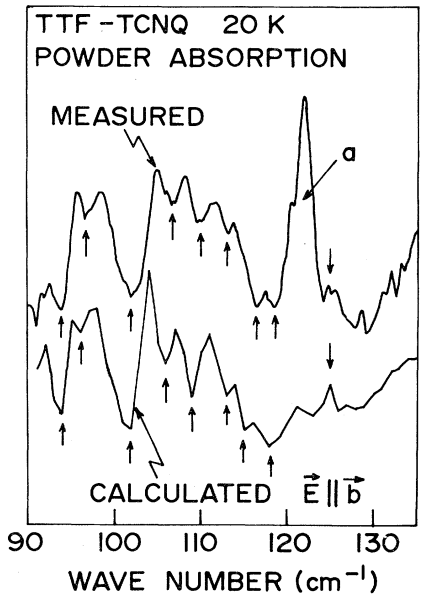

FIG. 9. Detailed portion of the spectra shown in Fig. 8.

with $g/\epsilon_m = \frac{1}{1000}$. Notice the broad peak at 315 cm^{-1} together with the medium dip at 260 cm^{-1} and the very shallow dip at 240 cm^{-1}. In contrast to the lower-wave-number features, these latter features are *peaks* in the conductivity, and therefore dips in the reflectivity and absorption coefficient. The 260-cm^{-1} dip is due to a TCNQ mode and the 240-cm^{-1} dip is due to a TTF mode.[3] The apparent peak between these two modes, at 253 cm^{-1}, was taken as an absorption peak by Bozio and Pecile.[9] The broad 315-cm^{-1} feature was assigned by them to be

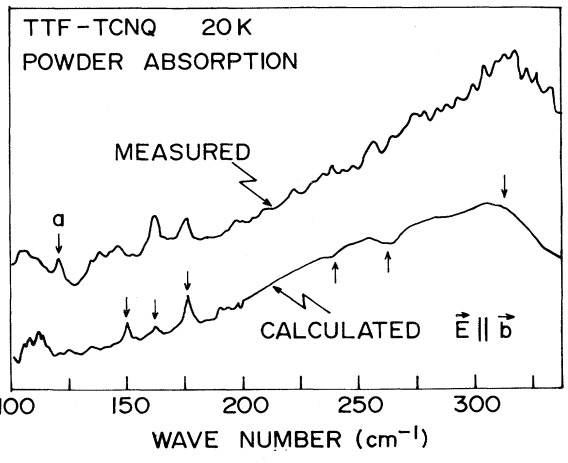

FIG. 10. High-wave-number range of our powder measurements on TTF-TCNQ at 20 K. Measured spectrum is $\ln(I_0/I)$. Calculated spectrum was obtained from Eqs. (8)—(10) with $g/\epsilon_m = \frac{1}{1000}$ and $f=0.05$. 120-cm^{-1} $\vec{E}||\vec{a}$ feature is indicated. $\vec{E}||\vec{b}$ features common to the two spectra are also indicated. Two spectra have been vertically displaced for ease of comparison.

another TCNQ mode, $\nu_9(a_g)$, whereas we feel it may be an indication of the band edge. This would disappear at the insulator-metal transition, as it is observed to do, just as an activated vibration would. Etemad[8] chose to assign the dip at 340 cm^{-1} following this broad peak, seen more clearly in Fig. 7, to an activated vibration (of TTF in this case). Again the same comment applies.

It may be mentioned at this point that the large 290-cm^{-1} conductivity peak of Ref. 1 would be very noticeable in the powder spectra of Fig. 10. The shape and magnitude of the powder spectrum above our region of interest depends very much on the filling factor and the medium, as well as the size of powder particles and thickness of the samples. Furthermore, the simplified theory used here involves some assumptions which are not valid at high wave numbers. Small-particle scattering and retardation effects[20] must also be considered. It is therefore difficult to calculate the powder absorption seen by other workers at higher wave numbers.

IV. $\vec{E}||\vec{b}$ ACTIVATED VIBRATIONS

In our recent vibrational analysis[3] of the bolometric spectra of TTF-TCNQ we found features for $\vec{E}||\vec{b}$ which had isotope shifts corresponding to the following: librations about the long axis of the molecules (z axis), a strong quartet due to TTF with the same isotope shifts as a z libration but which we assigned to $\nu_{10}(a_u)$, a torsion about the central bond, acoustic-lattice vibrations, totally symmetric gerade vibrational modes, and nontotally symmetric gerade vibrational modes. All of these resonances are infrared inactive in the undistorted phase of TTF-TCNQ [except for $\nu_{10}(a_u)$, which should be weak]. The lack of symmetry caused by the Peierls distortion could activate them but they would still be very weak. Since they are all so strong they must be coupling with the CDW, obtaining the associated electronic oscillator strength. Of the above types of vibration only the totally symmetric gerade modes are commonly seen as a result of a periodic lattice distortion and a CDW. We reasoned, therefore, that if the above vibrational modes were indeed becoming infrared activated, it may be because they represent a component of the distortion itself. The bolometric technique is a low-temperature technique and we were therefore unable to monitor the temperature dependence of these features at that time. The present powder spectra now allow us to do that.

Figure 11 shows the lower-wave-number portion of the spectrum at several temperatures. Nine features which are known to be $\vec{E}||\vec{b}$ have been indicated and numbered. All of them may be seen to have strong temperature dependences, as predicted. Feature 1 was tentatively assigned to an activated acoustic-lattice mode (see Table 2 in Ref. 3). Its disappearance by 51 K confirms the low-temperature activation. Feature 2 is a result of the small-particle "cutoff," best visualized in Fig. 7. Although reduced, it is still present at 51 K, as one would expect. Features 3—5 were assigned to mixed lattice modes involving R_z librations. Their disappearance at the insulator-metal transition also confirms their activation. Feature 6 is the TTF *quartet*

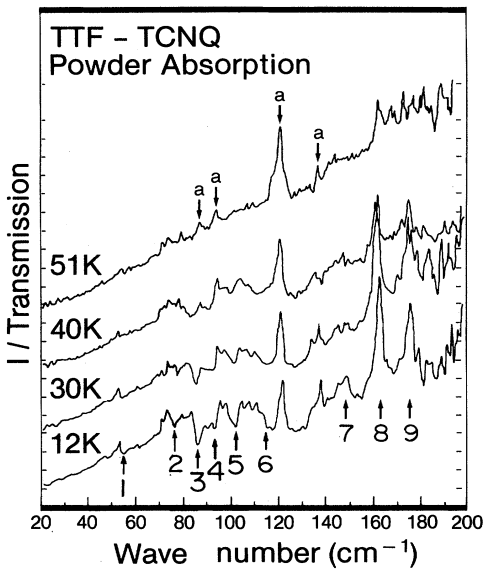

FIG. 11. Measured powder spectra of TTF-TCNQ at four temperatures. Nine distinct $\vec{E}||\vec{b}$ features are indicated with a number and referred to in the text. $\vec{E}||\vec{a}$ features are indicated as such. Resolution is 1 cm^{-1}.

which we assigned to $\nu_{10}(a_u)$. This may be seen more clearly in Fig. 12 with each component indicated. We have proposed that the quartet was a result of "zone folding" due to the $4\vec{a}$ periodicity of the Peierls distortion

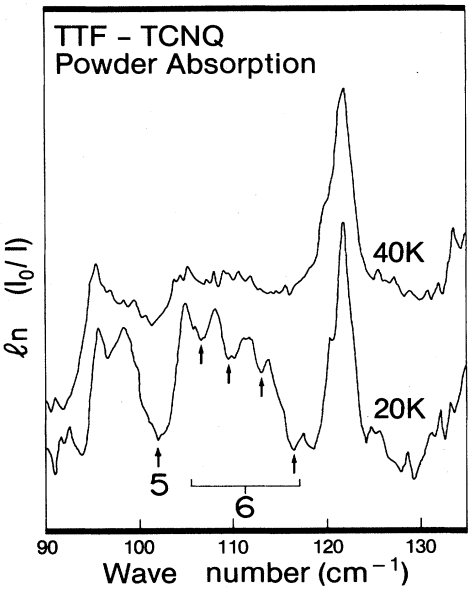

FIG. 12. Detailed portion of the powder spectrum of TTF-TCNQ at 20 and 40 K showing the TTF quartet assigned to $\nu_{10}(a_u)$, indicated as feature 6, and feature 5 which is thought to be a mixed lattice mode involving an R_z libration of the TTF molecule. The quartet is gone at 40 K, just above the 38-K transition temperature for the $4\vec{a}$ periodicity of the Peierls distortion.

below 38 K. The fact that the quartet is gone by 40 K, whereas the activated mixed mode (feature 5) is still present up to the insulator-metal transition, supports our interpretation. Returning to Fig. 11, features 7, 8, and 9 were assigned to TTF $\nu_{21}(b_{2g})$, TCNQ $\nu_{10}(a_g)$, and TCNQ $\nu_{31}(b_{2g})$, respectively. TTF $\nu_{21}(b_{2g})$ (feature 7) is very small by 40 K and is gone by 51 K. The activated TCNQ modes are seen more clearly in Fig. 13. TCNQ $\nu_{10}(a_g)$ (feature 8) is weak but still visible at 71 K (the 181-K spectrum is somewhat noisy), while TCNQ $\nu_{31}(b_{2g})$ (feature 9) is very small at 60 K and gone by 71 K. These findings are consistent with the view of one-dimensional fluctuating distortions on the TCNQ chains above the metal-insulator transition and the development of the TTF distortion below 49 K. The proximity of some of the features make it difficult to present detailed integrated-intensity—versus—temperature plots as we have recently done for the $\vec{E}||\vec{a}$ spectrum.[21]

V. CONCLUSION

In conclusion, we have used the bolometric technique to indirectly obtain the reflectivity of TTF-TCNQ at 12 K for radiation polarized along the chain axis $\vec{E}||\vec{b}$. Since R is so close to unity for $\vec{E}||\vec{b}$, our measurement of $1-R$ gave us detailed, high-resolution structure in R which would be very difficult to detect by direct means. A Kramers-Kronig analysis has been used to give the optical properties. The resulting conductivity spectrum is unusual. A very strong resonance at 35 cm^{-1} has been attributed to the phase mode of the pinned CDW, in agreement with Tanner *et al.*[1] This is followed by a strong broad conductivity feature in the semiconducting gap below 315 cm^{-1} starting with a gentle edge just above 100 cm^{-1}. This conductivity is higher than that above the semiconducting gap, rendering chemical impurities unlikely candidates responsible for much of the midgap conductivity. A possible explanation in terms of solitons and the higher-order breather modes, of which the phase mode of the pinned CDW is the first, has been suggested. We attribute the very large peak at 290 cm^{-1} found by Tanner *et al.*[1] to inaccuracies in their absolute value of R.

We have confirmed the optical properties obtained by comparing the structure in the calculated absorption coefficient with that which we have measured using very fine powders. The agreement is very good. The most important parameter is the magnitude of small-particle effects, which severely reduces the absorption coefficient below a cutoff wave number. Reasonable effects are observed for both our powder measurements and previous thin-film results. It has been shown that these effects mask the pinned CDW and falsely indicate a semiconducting gap at all temperatures. $\vec{E}||\vec{a}$ features are also seen to be prominent in the powder spectra, even though their conductivities are very small compared with $\vec{E}||\vec{b}$ features. This is because their absorption coefficients are comparable.

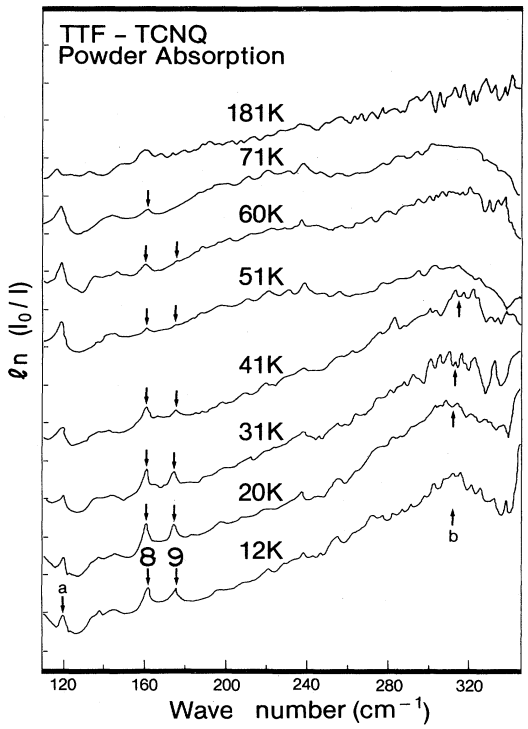

FIG. 13. Measured powder spectra of TTF-TCNQ at eight temperatures. Two $\vec{E}||\vec{b}$ features labeled 8 and 9 are referred to in the text. Broad $\vec{E}||\vec{b}$ feature at 315 cm^{-1} is also indicated, as well as the 120-cm^{-1} $\vec{E}||\vec{a}$ lattice mode. Resolution is 2 cm^{-1}.

Finally we have used the powder spectra to follow the $\vec{E}||\vec{b}$ vibrational features as the temperature is raised through the insulator-metal transition. All of the features are reduced and eventually disappear, but not all at the same rate. This confirms the activated nature of these vibrations which are coupling with the CDW at low temperatures. These vibrations include acoustic modes, mixed lattice modes, R_z librations, normally weak infrared modes such as $\nu_{10}(a_u)$, which is a torsion about the central bond of the TTF molecule, and normally infrared-inactive gerade modes of both molecules, including both totally symmetric a_g modes and non-totally-symmetric b_{2g} modes. We feel that these modes represent a component of the Peierls distortion at low temperatures.

ACKNOWLEDGMENT

This work was supported by Grant No. A5653 from the Natural Sciences and Engineering Research Council of Canada.

[1]D. B. Tanner, K. D. Cummings, and C. S. Jacobsen, Phys. Rev. Lett. 47, 597 (1981).
[2]J. E. Eldridge and F. E. Bates, Solid State Commun. 30, 195 (1979).
[3]Frances E. Bates, J. E. Eldridge, and M. R. Bryce, Can. J. Phys. 59, 339 (1981).
[4]J. E. Eldridge, Solid State Commun. 26, 243 (1978).
[5]J. E. Eldridge, Solid State Commun. 21, 737 (1977).
[6]J. E. Eldridge, Solid State Commun. 19, 607 (1976).
[7]D. B. Tanner, C. S. Jacobsen, A. F. Garito, and A. J. Heeger, Phys. Rev. B 13, 3381 (1976).
[8]Shahab Etemad, Phys. Rev. B 24, 4959 (1981).
[9]R. Bozio and C. Pecile, Solid State Commun. 37, 193 (1981).
[10]L. B. Coleman, C. R. Fincher, Jr., A. F. Garito, and A. J. Heeger, Phys. Status Solidi B 75, 239 (1976).
[11]C. S. Jacobsen, Ph.D. thesis, Technical University of Denmark, 1975 (unpublished), p. 92.
[12]In Ref. 5, in which one of the present authors suppressed the bolometric response in order to increase the photoconductive response, a decrease by a factor of 25 in the signal above 300 cm^{-1} was obtained. The signal curves obtained under these conditions were *scaled* in Figs. 1 and 2 of Ref. 5 to match the bolometric spectra at 600 cm^{-1}.
[13]P. M. Grant, R. L. Greene, G. C. Wrighton, and G. Castro, Phys. Rev. Lett. 31, 1311 (1973).
[14]G. Anderman, A. Caron, and David A. Dows, J. Opt. Soc. Am. 55, 1210 (1965).
[15]M. J. Rice, A. R. Bishop, J. A. Krumhansl, and S. E. Trullinger, Phys. Rev. Lett. 36, 432 (1976).
[16]A. J. Berlinsky, Rep. Prog. Phys. 42, 1243 (1979).
[17]R. K. Bullough and P. J. Caudrey, in *Solitons,* Vol. 17 of *Topics in Current Physics,* edited by R. K. Bullough and P. J. Caudrey (Springer, New York, 1980), p. 1.
[18]E. Mendel and A. J. Berlinsky (private communication).
[19]The only unusual feature is the fairly strong one at 163 cm^{-1} [$\nu_{10}(a_g)$], which is calculated to be weak for $\vec{E}||\vec{b}$ and is also very weak in the $\vec{E}||\vec{a}$ spectrum relative to the 120-cm^{-1} feature.
[20]C. G. Grangvist and O. Hunderi, Phys. Rev. B 16, 3513 (1977).
[21]J. E. Eldridge and F. E. Bates, Phys. Rev. B 26, 1590 (1982).